

PAPER • OPEN ACCESS

## Advanced iontronic spiking modes with multiscale diffusive dynamics in a fluidic circuit

To cite this article: T M Kamsma *et al* 2024 *Neuromorph. Comput. Eng.* **4** 024003

View the [article online](#) for updates and enhancements.

### You may also like

- [Soft iontronic delivery devices based on an intrinsically stretchable ion selective membrane](#)  
Dennis Cherian, Samuel Lienemann, Tobias Abrahamsson et al.
- [A tutorial of characterization methods on flexible pressure sensors: fundamental and applications](#)  
Yongbiao Wan, Zhiguang Qiu, Jun Yuan et al.
- [Frequency dependent sensitivity of hydrogel iontronic sensor](#)  
Haiyang Liu, Haoyu Guo, Meng Yang et al.



## PAPER

## OPEN ACCESS




RECEIVED  
26 January 2024REVISED  
11 April 2024ACCEPTED FOR PUBLICATION  
19 April 2024PUBLISHED  
30 April 2024

Original Content from  
this work may be used  
under the terms of the  
[Creative Commons  
Attribution 4.0 licence](#).

Any further distribution  
of this work must  
maintain attribution to  
the author(s) and the title  
of the work, journal  
citation and DOI.



## Advanced iontronic spiking modes with multiscale diffusive dynamics in a fluidic circuit

T M Kamsma<sup>1,2,\*</sup> , E A Rossing<sup>1</sup>, C Spitoni<sup>2</sup>  and R van Roij<sup>1,\*</sup> <sup>1</sup> Institute for Theoretical Physics, Utrecht University, Princetonplein 5, 3584 CC Utrecht, The Netherlands<sup>2</sup> Mathematical Institute, Utrecht University, Budapestlaan 6, 3584 CD Utrecht, The Netherlands

\* Authors to whom any correspondence should be addressed.

E-mail: [t.m.kamsma@uu.nl](mailto:t.m.kamsma@uu.nl) and [r.vanroij@uu.nl](mailto:r.vanroij@uu.nl)**Keywords:** iontronic spiking, ion channel memristor, microfluidic circuit, tonic bursting, phasic bursting, mixed mode spiking, threshold variabilitySupplementary material for this article is available [online](#)**Abstract**

Fluidic iontronics is emerging as a distinctive platform for implementing neuromorphic circuits, characterised by its reliance on the same aqueous medium and ionic signal carriers as the brain. Drawing upon recent theoretical advancements in both iontronic spiking circuits and in dynamic conductance of conical ion channels, which form fluidic memristors, we expand the repertoire of proposed neuronal spiking dynamics in iontronic circuits. Through a modelled circuit containing channels that carry a bipolar surface charge, we extract phasic bursting, mixed-mode spiking, tonic bursting, and threshold variability, all with spike voltages and frequencies within the typical range for mammalian neurons. These features are possible due to the strong dependence of the typical conductance memory retention time on the channel length, enabling timescales varying from individual spikes to bursts of multiple spikes within a single circuit. These advanced forms of neuronal-like spiking support the exploration of aqueous iontronics as an interesting platform for neuromorphic circuits.

**1. Introduction**

In the pursuit of brain-inspired circuits the focus is often on the synaptic properties of neuromorphic devices, where synapses are considered as primary computational units in neuromorphic computing [1]. Consequently, due to their analogous behaviour to synapses, memristors have significantly shaped and driven research in this domain, where the time- and history-dependent conductance of memristors offers a versatile platform for emulating features of synaptic plasticity [2–4]. However, synapses are not the only components in the brain which can be emulated with memristors. The biological ion channels responsible for generating action potentials also exhibit memristive behaviour [5]. This is underscored by the seminal Hodgkin–Huxley (HH) model [6], which mathematically describes the axonal membrane potential by treating the membrane as an equivalent electric circuit in which the ion channels embedded in the axonal membrane are modelled as circuit components. The mathematical models for these ion channels were later recognised as descriptions of memristors [7]. Although both synapses and axonal ion channels are neuronal components that can be described and emulated by memristors, they are explicitly distinct biological structures which carry out different tasks. This biological nuance sometimes leads to confusion and inaccurate descriptions of memristive devices in the brain, such as incorrectly associating the HH model with descriptions of synapses [8]. Nevertheless, the intriguing connection between memristors and the HH model has also sparked considerable interest [5, 9] and neuronal signalling has inspired various circuits that capture various features of neuronal spiking [10, 11].

Biological neurons feature a wealth of different spiking modes, which can be clearly categorised and used to judge the quality of neuron models [12]. Typically the most basic features to consider are *tonic spiking*, a regular train of voltage spikes with constant frequency, and *phasic spiking*, a single isolated voltage spike. In

the case of phasic spiking, the neuron model should also obey the all-or-none law [4, 13], i.e. a voltage spike is either fully generated upon a sufficiently strong impulse, or the voltage fails to spike, with no intermediate transition in between. However, many more neuronal firing modes are recognised and this signalling behaviour of neurons has inspired various circuits that can emulate a wide array of different modes of neuronal spiking [10, 11]. Examples, that will also feature in the present study, include *phasic bursting*, *mixed mode spiking*, *tonic bursting* (otherwise known as *chattering* [14]), and *threshold variability* [12]. In phasic bursting, a single burst of several spikes emerges upon applying a sustained stimulus, after which the system again settles to a steady state, despite the constant and sustained current stimulus. Mixed mode spiking consists of an initial burst of spikes upon a sustained stimulus, followed by tonic spiking. In tonic bursting, short periods of spiking, i.e. bursts, are interchanged by short periods of no spiking at all. Lastly, threshold variability indicates that the threshold for a neuron to spike can depend on the prior activity of the neuron.

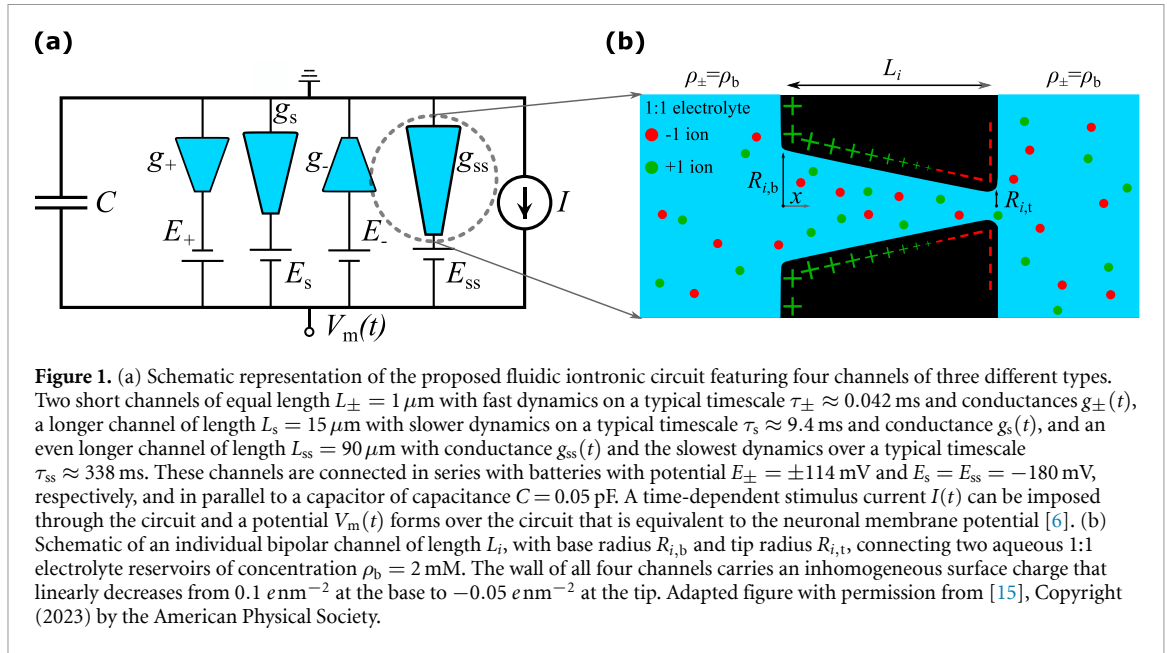
The vast majority of neuromorphic devices (both spiking and synaptic) consist (at least partially) of solid-state components [2, 3, 10, 11], which results in fundamental differences with biological neurons. For instance, while solid-state devices typically rely on a single information carrier, such as electrons or holes, driven only by electric forces, neurons employ the transport of various ions and molecules in parallel, while combining electrical and chemical regulation, both for signalling [16] and for synaptic transmission [17–19]. Additionally, the fast dynamics of solid state components can be a disadvantage when temporal inputs are natural or biological signals as the typical timescales of those inputs can be significantly slower than those of solid-state devices, therefore requiring complicated virtual clocks for synchronisation [20, 21]. Recent work tries to address and overcome these limitations through electrochemical coupling of solid-state components to ionic systems, both in the context of synaptic devices [22, 23] and for spiking circuits [24–26]. However, a newly emerging direction proposes to omit solid-state components altogether, and hence the need for any chemical or ionic coupling, by implementing neuromorphic features in an aqueous electrolyte medium [27–34]. These (fluidic) iontronic devices have recently garnered significant interest, offering the promise of multiple information carriers, chemical regulation, and bio-integrability [35], although sacrificing on the high speeds obtainable by solid state devices. Unlike traditional solid-state neuromorphic circuits, fluidic iontronic circuits leverage the dynamic interplay of ions within an aqueous electrolyte, mirroring the conductive and fluidic characteristics inherent in biological neuronal environments. This departure from solid-state components introduces a novel dimension to neuromorphic computing, offering the potential for closer emulation of the brain's aqueous dynamics [36, 37]. Recent advances include chemical regulation [30, 31] and initial demonstrations of iontronic neuromorphic computing [38]. However, the development of neuromorphic iontronic devices is still in its infancy, requiring further theoretical explorations and experimental investigations to establish their capabilities in emulating complex neuronal functionalities [28, 34, 35].

In the recent rise of interest in iontronic neuromorphics, spiking circuits also received some attention in the form of theoretical studies, where HH-inspired iontronic circuits are modelled and shown to exhibit features of neuronal spiking [15, 29]. These proposals feature a circuit composed of an aqueous electrolyte medium, akin to the neuronal medium that the HH model describes, and rely on fluidic iontronic memristors to induce neuronal spiking. Initially, tonic spiking was shown to emerge from a circuit containing Angstrom-scale slits [29], shortly after which an alternative iontronic circuit exploiting conical ion channels was proposed that exhibits both the characteristic all-or-none phasic spiking and tonic spiking [15]. Thus, the two modes that are typically considered first [11, 12] have been theoretically predicted to also emerge from fluidic iontronic circuits. However, no proposals yet exist to also include other spiking modes.

In this work we expand upon the previously reported features of neuronal spiking in fluidic iontronics [15, 29]. By building upon a previously reported iontronic circuit [15] and a physical description of the dynamical conductance of conical channels with a bipolar (BP) surface charge [39], i.e. positive at the base and negative at the tip, we can unlock various new forms of spiking dynamics. Due to the strong dependence of the typical conductance memory retention time on the channel length, we can implement timescales varying from individual spikes to bursts of multiple spikes within a single circuit, thereby enabling new spiking modes. Specifically these spiking modes are the aforementioned phasic bursting, mixed mode spiking, tonic bursting, and threshold variability [12].

## 2. Iontronic circuit and BP channels

Conical fluidic ion channels act as iontronic volatile memristors [40] and are being investigated as possible candidates for synaptic devices [41] and spiking circuits [15, 39]. Using theoretical models that quantitatively explain the memristive behaviour of conical channels, it was shown that HH-inspired fluidic circuits containing three conical channels and a capacitor exhibit tonic and phasic spiking [15, 39]. This modelled circuit was originally composed of conical ion channels with a homogeneous unipolar (UP) surface charge



[15] and was later modified by replacing the UP channels with conical channels carrying a BP inhomogeneous surface charge [39], positive at the base and negative at the tip. BP fluidic channels and (Janus) membranes have long drawn great interest as current rectifiers [42–47] for applications in e.g. sensing [47] and osmotic energy conversion [47–49]. BP channels also show potential for iontronic memristors as a modification from a UP to a BP surface charge led, for an individual conical channel, to a much more pronounced current–voltage hysteresis loop upon applying an AC voltage, i.e. a stronger conductance memory effect.

Here we consider a circuit containing several of these conical BP channels, with different lengths  $L_i$ . An important feature of these BP channel memristors is that their typical conductance memory timescale is dictated by the channel lengths  $L_i$  according to

$$\tau_i = \frac{L_i^2}{12D}, \quad (1)$$

with  $D = 2 \mu\text{m}^2 \text{ ms}^{-1}$  the diffusion coefficient of the ions [39], which we assume to be identical for all ionic species for convenience. As we will discuss in section 3.6, the combination of channels of various lengths in a single circuit gives rise to dynamics on the timescale of individual spikes and of bursts of spikes.

To unlock additional features of neuronal firing, beyond tonic and phasic spiking, we introduce the circuit schematically depicted in figure 1(a), containing a capacitor with capacitance  $C = 0.05 \text{ pF}$ , a typical capacitance for a mammalian neuronal membrane with an area of order  $\sim 0.1 \mu\text{m}^2$  [50, 51], i.e. of the same order as the cross-sectional area of a channel. This capacitor is connected in parallel with four BP conical channels with conductances  $g_+(t)$ ,  $g_-(t)$ ,  $g_s(t)$ , and  $g_{ss}(t)$ , and four batteries each in series with the conical channels. The channels are taken to be of varying lengths  $L_{\pm} = 1 \mu\text{m}$ ,  $L_s = 15 \mu\text{m}$ , and  $L_{ss} = 90 \mu\text{m}$ . Through equation (1) this translates to timescales  $\tau_{\pm} \approx 0.042 \text{ ms}$  for the two fast channels,  $\tau_s \approx 9.4 \text{ ms}$  for the slow channel, and  $\tau_{ss} \approx 338 \text{ ms}$  for the super slow channel. The batteries have potentials  $E_{\pm} = \pm 114 \text{ mV}$  for the two fast channels, and  $E_s = E_{ss} = -180 \text{ mV}$  for the slow and super slow channels. These batteries, which mimic the Nernst potential caused by ionic concentration differences inside and outside the neuron in the HH model [6], are considered to be actual batteries in the microfluidic circuit of interest here, but their potentials are comparable to their biological Nernst potential counterparts [52].

In figure 1(b) we show a schematic depiction of a BP channel of length  $L_i$ , implemented in the circuit in figure 1(a), with base- and tip radii  $R_{i,b}$  and  $R_{i,t} = R_{i,b} - \Delta R_i$ , respectively, and thus with radius  $R_i(x) = R_{i,b} - x\Delta R_i/L_i$  for positions  $x \in [0, L_i]$  in the channel. The channel connects two 1:1 aqueous electrolyte reservoirs with the viscosity  $\eta = 1.01 \text{ mPa} \cdot \text{s}$  and the electric permittivity  $\varepsilon = 0.71 \text{ nF} \cdot \text{m}^{-1}$  of water. The cationic and anionic bulk concentrations are given by  $\rho_b = 2 \text{ mM}$ , comparable to the extracellular potassium concentration in biological neurons [52], which gives rise to a Debye length  $\lambda_D \approx 6.8 \text{ nm}$ . The channels carry a surface charge that linearly decreases from  $e\sigma_0 = 0.1 \text{ e nm}^{-2}$  at the broad base to  $-0.05 \text{ e nm}^{-2}$  at the narrow tip, thereby changing by  $\sigma' = -3\sigma_0/2$  over the channel length and forming a BP surface charge profile. These charge densities correspond to Gouy–Chapman zeta potentials that vary

between 92 mV and  $-61$  mV. For the short fast channels and the slow channel we fix  $R_{i,b} = 200$  nm and  $R_{i,t} = 50$  nm, while the super slow channel is narrower with  $R_{ss,b} = 120$  nm and  $R_{ss,t} = 30$  nm. Thus, in all cases the channel radii are substantially larger than the Debye length, such that overlap of electric double layers is not prominent.

To fully resolve the dynamics of the circuit depicted in figure 1(a), we have to know how the conductances  $g_i(t)$  of the BP channels evolve. For this we use an analytical model that quantitatively describes the steady-state and dynamical conductance properties of BP channels [39]. BP channels exhibit voltage-dependent salt concentration polarisation in steady-state, with the radially averaged salt concentration  $\bar{\rho}_{i,s}(x, V_i)$  described by

$$\bar{\rho}_{i,s}(x, V_i) = 2\rho_b - \frac{1}{\text{Pe}_i(V_i)/V_i} \frac{2e(\sigma_0\Delta R_i + \sigma'R_{i,b})}{k_B T R_{i,t}^2} \left( \frac{R_{i,b}(1-x/L_i)}{R_i(x)} - \frac{e^{-\text{Pe}_i(V_i)\frac{(1-x/L_i)R_{i,t}}{R_i(x)} - 1}}{e^{-\text{Pe}_i(V_i)\frac{R_{i,t}}{R_{i,b}} - 1}} \right), \quad (2)$$

with  $\text{Pe}_i(V_i) = Q_i(V_i)L_i/(\pi DR_{i,t}^2)$  the Péclet number at the narrow end and  $Q_i(V_i) = -\pi R_{i,t}R_{i,b}\varepsilon\psi_{\text{eff}}V_i/(\eta L_i)$  the volume flow through the channel. The system is considered to be at a temperature of 293.15 K and the effective surface potential  $\psi_{\text{eff}} = -25$  mV is taken to be the same as in [39] as we consider the same surface charge distributions here. The accumulation or depletion of salt affects the conductance of the channel according to

$$g_{i,\infty}(V_i) = g_{i,0} \frac{L_i}{2\rho_b \int_0^{L_i} (\bar{\rho}_{i,s}(x, V_i))^{-1} dx}, \quad (3)$$

with  $g_{i,0} = (\pi R_{i,t}R_{i,b}/L_i)(2\rho_b e^2 D/k_B T)$  the homogeneous channel conductance. In the numerical evaluation of equation (3) we replace  $\bar{\rho}_{i,s}(x, V_i)$  by  $\text{Max}[0.2\rho_b, \bar{\rho}_{i,s}(x, V_i)]$  to avoid nonphysical negative concentrations that can emerge due to the strong voltage-dependent salt depletion of BP channels [39]. This approach does induce a sharper drop in conductance, compared to full finite-element simulations, when concentrations start to approach the imposed minimum of  $0.2\rho_b$ , discussed in more detail in the supplemental material. This artefact complicates the circuit equations we introduce below. To help smooth over this sharper drop we employ a third-order interpolation to evaluate equation (3) between voltages spaced at intervals of 0.025 V, ranging from  $-0.3125$  to  $0.3125$  V. A more sophisticated theoretical model of individual channels in the future should obviate the need for such an *ad hoc* approach, but for now this effective method suffices.

Since it takes a typical time  $\tau_i$  as per equation (1) for salt to accumulate or deplete, the channel exhibits a (volatile) memory conductance with typical memory retention time  $\tau_i$ . The resulting dynamic conductance  $g_i(t)$  was found to be well described by

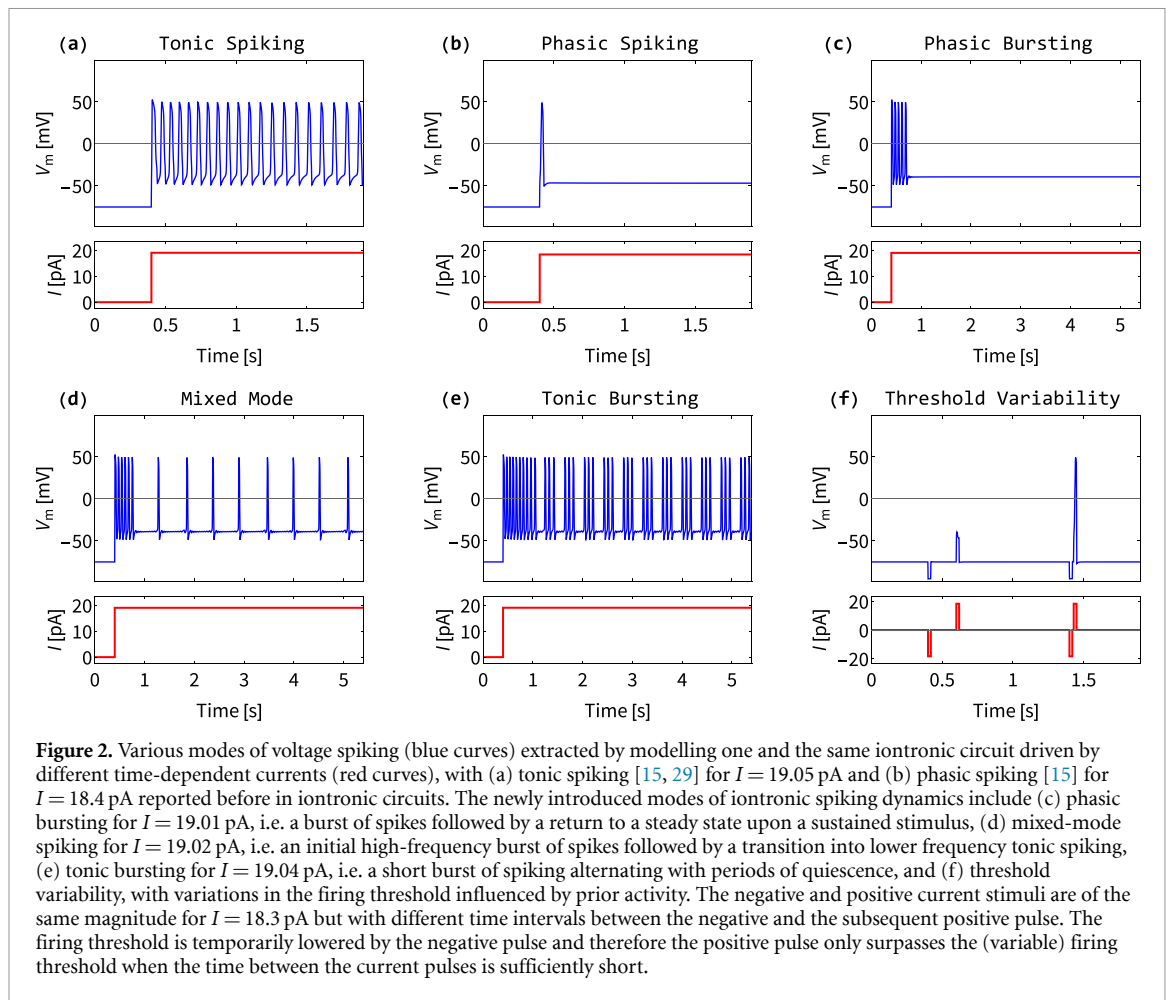
$$\frac{dg_i(t)}{dt} = \frac{g_{i,\infty}(V_i(t)) - g_i(t)}{\tau_i}, \quad (4)$$

where  $V_i(t)$  is the potential difference between base and tip of the channel,  $g_{i,\infty}(V_i)$  is the voltage-dependent steady-state conductance of the channel as per equation (3), and  $\tau_i$  is the typical conductance memory retention timescale of the channel given by equation (1) [39].

With differential equations for each of the dynamic conductances  $g_i(t)$ , we only need one additional equation to close the set that describes the time-evolution of the ‘membrane’ potential  $V_m(t)$ , here the potential over the capacitor. This additional equation is provided by Kirchhoff’s law

$$C \frac{dV_m(t)}{dt} = I(t) - \sum_i g_i(t) (V_m(t) - E_i), \quad (5)$$

where  $i \in \{+, -, s, ss\}$  and the conductances  $g_i(t)$  each evolve according to equation (4) with their corresponding  $g_{i,\infty}(V_i(t))$  and  $\tau_i$ . The voltage arguments  $V_i(t)$  over the channels are given by  $V_-(t) = V_m(t) - E_-$ ,  $V_+(t) = -V_m(t) + E_+$ ,  $V_s(t) = -V_m(t) + E_s$ , and  $V_{ss}(t) = -V_m(t) + E_{ss}$ , with the different signs of the potentials corresponding to the different orientations of the channels as depicted in figure 1(a). Using the initial conditions  $V(0) = -70$  mV and  $g_i(0) = g_{i,0}$ , with  $g_{i,0}$  as defined below equation (3), we numerically solve the closed set of equations (1), (4) and (5) for various current stimuli  $I(t)$ . The system is given at least 10 s to settle into a steady state before applying a current  $I(t)$ , we offset the time in the results to omit this in the plots.



Note that  $\tau_{\pm} \ll \tau_s, \tau_{ss}$ , additionally  $\tau_{\pm}$  is much faster than the typical response time of  $V_m(t)$  too as we will see later, so the two short channels actually act as quasi-instantaneous current rectifiers due to their comparatively fast dynamics, rather than memristors, as we will more extensively discuss in section 3.6.

### 3. Advanced iontronic spiking modes

Upon numerically evaluating the membrane potential  $V_m(t)$  that emerges from the proposed fluidic iontronic circuit introduced in section 2 for various stimuli, we reveal the remarkable diversity of typical neuronal firing modes [12] shown in figure 2, which we will discuss individually below. We stress that all spiking modes discussed below originate from one and the same iontronic circuit, with the stimulus current  $I(t)$  the only difference between the spiking modes. Additionally, we note that all spikes exhibit voltage amplitudes and spiking frequencies that are typical for mammalian neurons [13].

#### 3.1. Tonic spiking and phasic spiking

The earlier reported foundational tonic [15, 29] and phasic spiking [15] also emerge from the circuit we consider here. Tonic spiking, characterised by a regular train of voltage spikes as shown in figure 2(a), and phasic spiking, featuring a single isolated voltage spike as shown in figure 2(b), appear for the present system parameters under sustained current stimuli of 18.40 pA and 19.05 pA, respectively. The phasic spiking current stimulus of 18.40 pA is just above the threshold for any spiking to occur, unless we consider the variability of the threshold as discussed in section 3.5. The sustained current of figure 2(b) does give rise, after the single voltage pulse, to a steady voltage that differs from the initial voltage. An all-or-none spike can also appear upon a pulse stimulus, after which the voltage settles back to its initial steady-state [39].

The dynamics here are governed by the typical RC-like time of the circuit that determines the time it takes for the (de)polarisation of  $V_m(t)$ , while the timescale  $\tau_s$  dictates the typical width of a spike; the short channels respond on such fast timescales that their dynamics can be assumed to be instantaneous [15, 53]. Although the timescale  $\tau_{ss}$  does not play a role in these spiking modes as these also appear without the super slow channel [39], a small influence of the super slow channel is still visible in the case of tonic spiking. The



spiking frequency initially is slightly higher immediately after the stimulus is applied and then gradually settles into a lower frequency over a time  $\sim\tau_{ss}$ . This actually corresponds to the spiking mode of *spike frequency adaptation* [12], but since this effect is so minor in our results, we choose not to explicitly distinguish it as an additional emerging spiking mode.

### 3.2. Phasic bursting

Imposing a sustained current stimulus to the circuit of 19.01 pA elicits phasic bursting, a spiking mode where a burst of spikes occurs, followed by a return to a (new) steady state, despite the sustained stimulus. This mode is made possible by the super slow channel. The initial burst has a duration of the typical timescale  $\sim\tau_{ss}$  of the super slow channel, after which this channel has had sufficient time to increase its conductance to return the system to a steady state.

### 3.3. Mixed mode

Under a sustained stimulus of 19.02 pA we find mixed mode spiking, i.e. the iontronic circuit transitions from an initial high-frequency burst of spikes with a duration of  $\sim\tau_{ss}$ , into a lower frequency tonic spiking, with the individual spikes now separated by  $\sim\tau_{ss}$ , as shown in figure 2(d). In this case the initial burst is a transient, of typical time  $\sim\tau_{ss}$ , as the system settles into the periodic solution of the tonic spiking.

### 3.4. Tonic bursting

Tonic bursting entails short bursts of spiking interspersed with periods of quiescence. When imposing a sustained stimulus of 19.04 pA we find that the circuit exhibits a periodic behaviour of high frequency burst as shown in figure 2(e). The durations of the bursts and periods of quiescence are dictated by the slow dynamics of longest channel, as the super slow channel periodically increases and decreases in conductance, visible by the fact that each burst or quiescence period has a duration of order  $\sim\tau_{ss} \approx 338$  ms.

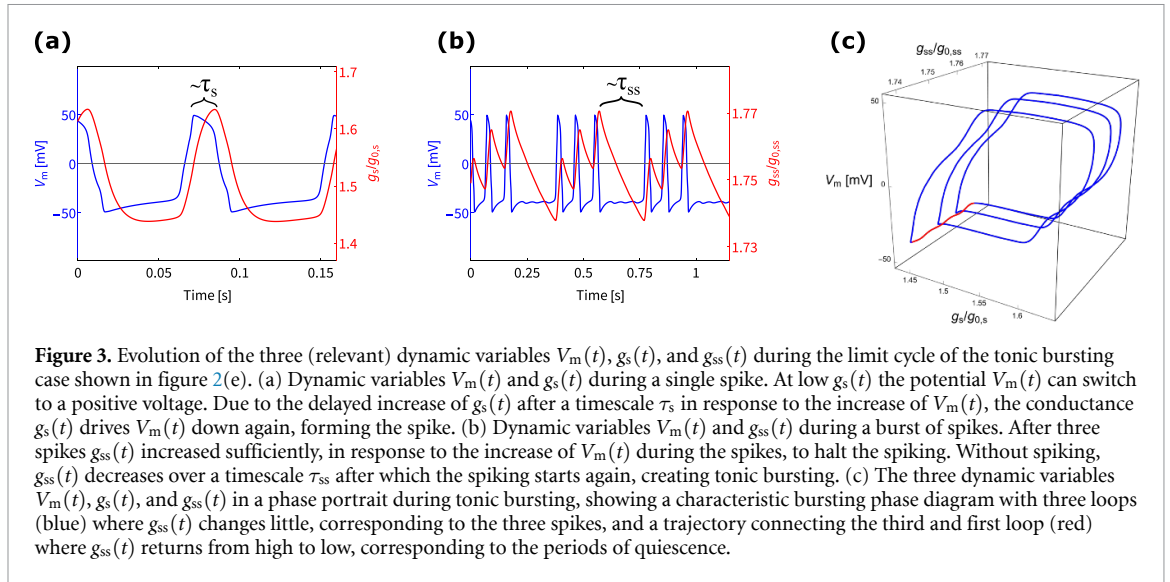
### 3.5. Threshold variability

Our findings also unveil threshold variability, wherein the firing threshold of the neuron is influenced by prior activity. As shown in figure 2(f), when imposing a negative and positive stimulus pulse of magnitude  $\pm 18.30$  pA (just below the threshold mentioned in section 3.1) of duration 0.02 s, separated by 0.18 s (between the end of the first pulse and the beginning of the second) no spike occurs. However, when we impose precisely the same pulses but now separated by 0.01 s we find that a full spike occurs. Thus in the first set of pulses, the threshold for spiking was not reached, but in the second instance it was reached with exactly the same pulses, showing that the prior activity of the circuit can influence the threshold for spiking. This is a result of the slow channel with timescale  $\tau_s$  decreasing in conductance as a result of the negative pulse, while the super slow channel actually plays no role in this spiking mode as it is also observed without the super slow channel. If the interval is much larger than  $\tau_s \approx 9.4$  ms, as it is for the first set of pulses, then the slow channel reverts to its steady-state before the second pulse. However, if the interval between the stimuli is of the order of  $\tau_s = 9.4$  ms (or smaller), as is the case in the second set of pulses where the interval is 10 ms, then the slow channel still has a lowered conductance when the second pulse arrives, making the system more susceptible to stimuli and thereby lowering the firing threshold.

### 3.6. Roles of the different channels

To elucidate the circuit design as shown in figure 1(b) we heuristically describe the roles the various channels play. Firstly, since  $\tau_{\pm}$  is much shorter than the typical response time of  $V_m(t)$  and since  $\tau_{\pm} \ll \tau_s, \tau_{ss}$ , the two short channels actually act as quasi-instantaneous current rectifiers, rather than memristors, though we solve the dynamic equation for all channels for completeness. Tonic and phasic spiking, which occur without the super slow channel, were already remarked to also emerge by using the instantaneous conductance  $g_{\infty, \pm}(V(t))$  [15] in equation (5), reducing such a three channel circuit to a two-dimensional dynamic system with dynamic variables  $V_m(t)$  and  $g_s(t)$  [53]. By extension the results we present here are represented by the three dynamic variables  $V_m(t)$ ,  $g_s(t)$ , and  $g_{ss}(t)$ . In figure 3 we show these dynamic variables during the tonic bursting shown in figure 2(e).

All channels drive  $V_m(t)$  toward their respective battery potentials. When  $V_m(t)$  is near  $E_{\pm}$  the respective corresponding short fast channel has a high conductance and maintains  $V_m(t)$  in that state, forming temporary stable states between which  $V_m(t)$  switches during spiking. The slow channel, which drives  $V_m(t)$  towards  $E_s = -180$  mV, is in a low conductance state when  $V_m(t)$  is negative, allowing  $V_m(t)$  to depolarise and switch to the positive voltage state upon a stimulus. Following the increase in  $V_m(t)$ , the slow channel increases in conductance over a timescale  $\tau_s$  as we show in figure 3(a), resulting in a consequent downward shift of  $V_m(t)$ . This behaviour analogously resembles the delayed activation of  $K^+$  channels in the HH model [6]. The super slow channel, operating over a timescale  $\tau_{ss}$ , plays a role akin to the slow channel. However, as



we show in figure 3(b), it takes several spikes for the super slow channel to sufficiently increase in conductance and drive  $V_m(t)$  towards its negative battery potential  $E_{ss} = -180$  mV, consequently suppressing spiking. The resulting period of quiescence lasts a time  $\sim \tau_{ss}$ , forming a bursting process. The salt accumulation and depletion underpinning the conductance change of the super slow channel bear similarity to the slow intracellular  $\text{Ca}^{2+}$  accumulation and depletion implicated in regulating bursting in biological neurons [54–56]. Combining the three relevant dynamic variables  $V_m(t)$ ,  $g_s(t)$ , and  $g_{ss}(t)$  in one phase portrait yields figure 3(c), revealing a characteristic bursting trajectory with three loops (blue) and a path connecting the third and first loop (red), corresponding to the three spikes and to the periods of quiescence, respectively.

#### 4. Discussion and conclusion

Previously reported fluidic iontronic circuits have demonstrated tonic spiking [15, 29] and phasic spiking [15]. In this study, we extend the repertoire of emergent spiking modes by introducing a new HH-like fluidic iontronic circuit, consisting of a capacitor and four iontronic memristors, that exhibits phasic bursting, mixed-mode spiking, tonic bursting, and threshold variability [12], as well as the earlier reported tonic and phasic spiking [15, 29]. The spikes in our proposed modes exhibit voltages and frequencies that align with those observed in mammalian neurons [13]. Moreover, the capacitance, battery potentials and salt concentration in the circuit are comparable to their biological counterparts [52]. Our theoretical framework builds upon a previously proposed iontronic circuit that exhibits tonic and phasic spiking [15] and a physical model for conical ion channels with a BP (rather than UP) surface charge [39]. These channels are memristive [39] and their typical conductance memory retention time is dependent on the channel length. By varying the lengths of the four channels we can incorporate timescales on the order of a single spike and of entire bursts in a single circuit, allowing for the spiking and bursting processes that emerge from one and the same circuit.

While our theoretical framework in principle is fully physical, a limitation is the parameter sensitivity of the system, at least for the system parameters we considered. The stimuli strengths that induce different spiking modes are only separated by  $\sim 0.01$ – $0.1$  pA on the scale of about 20 pA. Notably, if wider current stimuli intervals are found for spiking, then it is possible that *class 2 spiking* [12] can also be distinguished as a separate feature as the transitions in frequency seem to be discontinuous, but class 1 or 2 spiking is typically evaluated over varying stimuli intervals which in our case are too narrow to meaningfully investigate this. Additionally, although spiking was found to emerge for a wide range of different parameter configurations, the spiking is sensitive to small individual changes of the short fast channels or their respective batteries, where (at least one mode of) spiking only appeared in the tight interval  $E_{\pm} \in \pm [113, 114.8]$  mV. The short fast channels play no dynamic roles in the circuit, but rather act as instantaneous current rectifiers that create the stable voltage states between which  $V_m$  oscillates during spiking due to the dynamic switching of the (super) slow channel. Hence, no memristive properties are required for the short fast channels, which only offer a current rectification of around  $\approx 21$  [39], and other (perhaps better performing) diodic devices from the wide range of iontronic current rectifiers [57–61] could be considered. Although some devices can be



described by similar theoretical models as we use here [38, 61], our analysis is limited to devices for which we have an analytical quantitative model, but iontronic devices that lack such models are still feasible for experimental fabrication. For the (super) slow channels we do require the specific (length-dependent) volatile dynamics we find for the iontronic memristors of concern here, but in this case the system is far more stable against parameter shifts, thereby supporting the use of the (super) slow channels as described here. At least one mode of spiking emerges for changing a single parameter at a time in the range  $E_s \in [-200, -90]$  mV,  $E_{ss} \in [-450, -140]$  mV, while the capacitance can even span orders of magnitude  $C \in [10^{-6}, 10^{-1}]$  pF. Therefore, the three components that govern the circuit dynamics, i.e. the (super) slow channels and the capacitor, are relatively robust once the short fast channels are in order.

The above suggestion for future improvements using other fluidic devices is supported by the fact that the results presented here are already an expansion on results we derived earlier for simpler UP conical channels carrying a homogeneous surface charge. Tonic bursting also emerges from a similar circuit with UP channels, but with circuit parameters (i.e. higher battery potentials, lower salt concentration, lower capacitance) and spiking voltages that are further removed from their biological analogues. The results and specific parameters for the UP channel circuit are laid out in the supplemental material. The emergence of tonic bursting in a different circuit with different fluidic memristors shows that the bursting spiking modes we present are not inherently dependent on the BP conical channels we consider here. Therefore, possible further improvements can be achieved by considering fluidic iontronic devices with an even wider range of attainable conductances. However, this is an issue of individual device physics and here we mostly focused on the overall circuit architecture and the spiking modes it enables.

In summary, we have considerably expanded the range of spiking modes proposed to emerge from iontronic fluidic circuits, entailing phasic bursting, mixed-mode spiking, tonic bursting, and threshold variability. The alignment of the spikes in our results with typical mammalian neuronal voltages and frequencies, combined with various circuit parameters that are comparable to their biological counterparts, further supports the potential that fluidic iontronics carry for neuromorphic spiking circuits. Moreover, since these biologically realistic spikes emerge from a circuit that is based upon the same aqueous electrolyte medium as in neurons, a unique perspective is the future possible integration with biological systems. However, the present system is rather sensitive to stimulus strengths and other circuit parameters, especially in the short fast channels, a limitation that may be mitigated by implementing fluidic devices with a broader range of available conductances. Nevertheless, we showed that the multiscale diffusive timescales of fluidic iontronic memristors of different lengths facilitate a relatively simple circuit that exhibits various advanced modes of neuronal spiking. Consequently, this work contributes to the ongoing exploration of fluidic iontronics as a promising platform for neuromorphic circuits, providing theoretical insights and proposed applications, thereby paving the way for future advancements in this burgeoning field.

## Data availability statement

All data that support the findings of this study are included within the article (and any supplementary files).

## Acknowledgments

This work is part of the D-ITP consortium, a program of the Netherlands Organisation for Scientific Research (NWO) that is funded by the Dutch Ministry of Education, Culture and Science (OCW).

## ORCID iDs

T M Kamsma  <https://orcid.org/0000-0002-8898-8337>

C Spitoni  <https://orcid.org/0000-0003-0192-606X>

R van Roij  <https://orcid.org/0000-0002-2221-294X>

## References

- [1] Schuman C D, Kulkarni S R, Parsa M, Mitchell J P, Date P and Kay B 2022 Opportunities for neuromorphic computing algorithms and applications *Nat. Comput. Sci.* **2** 10–19
- [2] Sangwan V K and Hersam M C 2020 Neuromorphic nanoelectronic materials *Nat. Nanotechnol.* **15** 517–28
- [3] Schuman C D, Potok T E, Patton R M, Birdwell J D, Dean M E, Rose G S and Plank J S 2017 A survey of neuromorphic computing and neural networks in hardware (arXiv:1705.06963)
- [4] Zhu J, Zhang T, Yang Y and Huang R 2020 A comprehensive review on emerging artificial neuromorphic devices *Appl. Phys. Rev.* **7** 011312
- [5] Sah M P, Kim H and Chua L O 2014 Brains are made of memristors *IEEE Circuits Syst. Mag.* **14** 12–36

- [6] Hodgkin A L and Huxley A F 1952 A quantitative description of membrane current and its application to conduction and excitation in nerve *J. Physiol.* **117** 500
- [7] Chua L, Sbitnev V and Kim H 2012 Hodgkin-Huxley axon is made of memristors *Int. J. Bifurcation Chaos* **22** 1230011
- [8] Caravelli F and Carbajal J P 2018 Memristors for the curious outsiders *Technologies* **6** 118
- [9] Chua L 2013 Memristor, Hodgkin-Huxley and edge of chaos *Nanotechnology* **24** 383001
- [10] Thakur C S et al 2018 Large-scale neuromorphic spiking array processors: a quest to mimic the brain *Front. Neurosci.* **12** 353526
- [11] Yang J-Q et al 2020 Neuromorphic engineering: from biological to spike-based hardware nervous systems *Adv. Mater.* **32** 2003610
- [12] Izhikevich E M 2004 Which model to use for cortical spiking neurons? *IEEE Trans. Neural Netw.* **15** 1063–70
- [13] Bean B P 2007 The action potential in mammalian central neurons *Nat. Rev. Neurosci.* **8** 451–65
- [14] Gray C M and McCormick D A 1996 Chattering cells: superficial pyramidal neurons contributing to the generation of synchronous oscillations in the visual cortex *Science* **274** 109–13
- [15] Kamsma T M, Boon W Q, Ter Rele T, Spitoni C and Van Roij R 2023 Iontronic neuromorphic signaling with conical microfluidic memristors *Phys. Rev. Lett.* **130** 268401
- [16] Micu I, Plemel J R, Capriarello A V, Nave K A and Stys P K 2017 Axo-myelinic neurotransmission: a novel mode of cell signalling in the central nervous system *Nat. Rev. Neurosci.* **19** 49–58
- [17] Pereda A E and Purpura D P 2014 Electrical synapses and their functional interactions with chemical synapses *Nat. Rev. Neurosci.* **15** 250–63
- [18] Xia Z and Storm D R 2005 The role of calmodulin as a signal integrator for synaptic plasticity *Nat. Rev. Neurosci.* **6** 267–76
- [19] Lüscher C and Malenka R C 2012 NMDA receptor-dependent long-term potentiation and long-term depression (LTP/LTD) *Cold Spring Harb. Perspect. Biol.* **4** 1–15
- [20] Covi E, Donati E, Liang X, Kappel D, Heidari H, Payvand M and Wang W 2021 Adaptive extreme edge computing for wearable devices *Front. Neurosci.* **15** 611300
- [21] Chicca E and Indiveri G 2020 A recipe for creating ideal hybrid memristive-CMOS neuromorphic processing systems *Appl. Phys. Lett.* **116** 120501
- [22] Wang Y et al 2022 Dynamic molecular switches with hysteretic negative differential conductance emulating synaptic behaviour *Nat. Mater.* **21** 1403–11
- [23] Van De Burgt Y, Melianas A, Keene S T, Malliaras G and Salleo A 2018 Organic electronics for neuromorphic computing *Nat. Electron.* **1** 386–97
- [24] Harikesh P C et al 2022 Organic electrochemical neurons and synapses with ion mediated spiking *Nat. Commun.* **13** 1–9
- [25] Harikesh P C et al 2023 Ion-tunable antiambipolarity in mixed ion-electron conducting polymers enables biorealistic organic electrochemical neurons *Nat. Mater.* **22** 242–8
- [26] Luo S et al 2023 Highly bionic neurotransmitter-communicated neurons following integrate-and-fire dynamics *Nano Lett.* **23** 4974–82
- [27] Noy A and Darling S B 2023 Nanofluidic computing makes a splash *Science* **379** 143–4
- [28] Noy A, Li Z and Darling S B 2023 Fluid learning: mimicking brain computing with neuromorphic nanofluidic devices *Nano Today* **53** 102043
- [29] Robin P, Kavokine N and Bocquet L 2021 Modeling of emergent memory and voltage spiking in ionic transport through Angstrom-scale slits *Science* **373** 687–91
- [30] Robin P et al 2023 Long-term memory and synapse-like dynamics in two-dimensional nanofluidic channels *Science* **379** 161–7
- [31] Xiong T et al 2023 Neuromorphic functions with a polyelectrolyte-confined fluidic memristor *Science* **379** 156–61
- [32] Emmerich T, Teng Y, Ronceray N, Lopriore E, Chiesa R, Chernev A, Artemov V, Di Ventra M, Kis A and Radenovic A 2023 Ionic logic with highly asymmetric nanofluidic memristive switches (arXiv:2306.07617)
- [33] Han S H, Kim S I, Oh M A and Chung T D 2023 Iontronic analog of synaptic plasticity: hydrogel-based ionic diode with chemical precipitation and dissolution *Proc. Natl Acad. Sci. USA* **120** e2211442120
- [34] Xie B, Xiong T, Li W, Gao T, Zong J, Liu Y and Yu P 2022 Perspective on nanofluidic memristors: from mechanism to application *Chem. Asian J.* **17** e202200682
- [35] Han S H, Oh M-A and Chung T D 2022 Iontronics: aqueous ion-based engineering for bioinspired functionalities and applications *Chem. Phys. Rev.* **3** 031302
- [36] Bocquet L 2023 Concluding remarks: iontronics, from fundamentals to ion-controlled devices-random access memories *Faraday Discuss.* **246** 618–622
- [37] Xiong T, Li W, Yu P and Mao L 2023 Fluidic memristor: bringing chemistry to neuromorphic devices *Innovation* **4** 100435
- [38] Kamsma T M, Kim J, Kim K, Boon W Q, Spitoni C, Park J and van Roij R 2023 Brain-inspired computing with fluidic iontronic nanochannels (arXiv:2309.11438v1)
- [39] Kamsma T M, Boon W Q, Spitoni C and van Roij R 2023 Unveiling the capabilities of bipolar conical channels in neuromorphic iontronics *Faraday Discuss.* **246** 125–40
- [40] Wang D, Kvetny M, Liu J, Brown W, Li Y and Wang G 2012 Transmembrane potential across single conical nanopores and resulting memristive and memcapacitive ion transport *J. Am. Chem. Soc.* **134** 3651–4
- [41] Ramirez P, Gómez V, Cervera J, Mafe S and Bisquert J 2023 Synaptical tunability of multipore nanofluidic memristors *J. Phys. Chem. Lett.* **14** 10930–4
- [42] Daiguji H, Oka Y and Shirono K 2005 Nanofluidic diode and bipolar transistor *Nano Lett.* **5** 2274–80
- [43] Vlassioux I and Siwy Z S 2007 Nanofluidic diode *Nano Lett.* **7** 552–6
- [44] Strathmann H, Krol J J, Rapp H J and Eigenberger G 1997 Limiting current density and water dissociation in bipolar membranes *J. Membr. Sci.* **125** 123–42
- [45] Montes De Oca J M, Dhanasekaran J, Córdoba A, Darling S B and De Pablo J J 2022 Ionic transport in electrostatic Janus membranes. an explicit solvent molecular dynamic simulation *ACS Nano* **16** 3768–75
- [46] Córdoba A, Montes De Oca J M, Dhanasekaran J, Darling Abd S B and De Pablo J J 2023 Current rectification by nanoparticles in bipolar nanopores *Mol. Syst. Des. Eng.* **8** 289
- [47] Huang X, Kong X-Y, Wen L, Jiang L, Huang X, Kong X-Y, Wen L and Jiang L 2018 Bioinspired ionic diodes: from unipolar to bipolar *Adv. Funct. Mater.* **28** 1801079
- [48] Yang H-C et al 2018 Janus membranes: creating asymmetry for energy efficiency *Adv. Mater.* **30** 1801495
- [49] Yan L, Yang X, Zhang Y, Wu Y, Cheng Z, Darling S B and Shao L 2021 Porous Janus materials with unique asymmetries and functionality *Mater. Today* **51** 626–47

- [50] Gentet L J, Stuart G J and Clements J D 2000 Direct measurement of specific membrane capacitance in neurons *Biophys. J.* **79** 314–20
- [51] Major G, Larkman A U, Jonas P, Sakmann B and Jack J J B 1994 Detailed passive cable models of whole-cell recorded CA3 pyramidal neurons in rat hippocampal slices *J. Neurosci.* **14** 4613–38
- [52] Squire L, Berg D, Bloom F, du Lac S, Ghosh A and Spitzer N 2008 *Fundamental Neuroscience* 3rd edn (Academic) ch 6
- [53] Kamsma T M, van Roij R and Spitoni C 2024 A simple mathematical theory for simple volatile memristors and their spiking circuits (arXiv:2404.08647)
- [54] Chay T R 1983 Eyring rate theory in excitable membranes: application to neuronal oscillations *J. Phys. Chem.* **87** 2935–40
- [55] Chay T R 1985 Chaos in a three-variable model of an excitable cell *Physica D* **16** 233–42
- [56] Xu Q, Tan X, Zhu D, Bao H, Hu Y and Bao B 2020 Bifurcations to bursting and spiking in the chay neuron and their validation in a digital circuit *Chaos Solitons Fractals* **141** 110353
- [57] Riza Putra B, Tshwenya L, Buckingham M A, Chen J, Jeremiah Aoki K, Mathwig K, Arotiba O A, Thompson A K, Li Z and Marken F 2021 Microscale ionic diodes: an overview *Electroanalysis* **33** 1398–418
- [58] Cheng L-J and Guo L J 2010 Nanofluidic diodes *Chem. Soc. Rev.* **39** 923–38
- [59] Lan W J, Edwards M A, Luo L, Perera R T, Wu X, Martin C R and White H S 2016 Voltage-rectified current and fluid flow in conical nanopores *Acc. Chem. Res.* **49** 2605–13
- [60] Kim J, Jeon J, Wang C, Chang G T and Park J 2022 Asymmetric nanochannel network-based bipolar ionic diode for enhanced heavy metal ion detection *ACS Nano* **16** 2189–97
- [61] Choi E, Wang C, Chang G T and Park J 2016 High current ionic diode using homogeneously charged asymmetric nanochannel network membrane *Nano Lett.* **16** 2189–97